

## Collisional and thermal ionization of sodium Rydberg atoms: II. Theory for $nS$ , $nP$ and $nD$ states with $n = 5–25$

K Miculis<sup>1</sup>, I I Beterov<sup>2</sup>, N N Bezuglov<sup>3</sup>, I I Ryabtsev<sup>2</sup>, D B Tretyakov<sup>2</sup>,  
A Ekers<sup>1,4</sup> and A N Klucharev<sup>3</sup>

<sup>1</sup> Institute of Atomic Physics and Spectroscopy, University of Latvia, LV-1586 Riga, Latvia

<sup>2</sup> Department of Quantum Electronics, Institute of Semiconductor Physics, 630090 Novosibirsk, Russia

<sup>3</sup> Fock Institute of Physics, St Petersburg State University, 198904 St Petersburg, Russia

<sup>4</sup> Department of Physics, University of Kaiserslautern, D-67663 Kaiserslautern, Germany

E-mail: [beterov@isp.nsc.ru](mailto:beterov@isp.nsc.ru)

Received 15 January 2005, in final form 4 April 2005

Published 26 May 2005

Online at [stacks.iop.org/JPhysB/38/1811](http://stacks.iop.org/JPhysB/38/1811)

### Abstract

A stochastic model of associative ionization in collisions of Rydberg atoms with ground-state atoms is presented. The conventional Duman–Shmatov–Mihajlov–Janev (DSMJ) model treats the ionization as excitation of Rydberg electron to the continuum by the electric-dipole field generated by exchange interaction within the quasi-molecular ion. The stochastic model essentially extends this treatment by taking into account redistribution of population over a range of Rydberg states prior to ionization, which is caused by non-adiabatic processes in overlapping multiple level crossings of quasi-molecular Rydberg states. The redistribution is modelled as diffusion of electrons in the Rydberg energy spectrum using a Fokker–Planck-type equation. The process of  $l$ -mixing of Rydberg states at large internuclear distances and twisting of the collision trajectories on attractive potentials are taken into account. The choice of the collision velocity distribution is also shown to be important. Associative ionization rates have been calculated for  $\text{Na}^{**}(nl) + \text{Na}$  collisions with  $n = 5–25$  and  $l = 0, 1, 2$ , and compared with the available experimental data and the calculations performed using the nonlinear DSMJ model. At relatively low  $n$  the stochastic model yields a substantially better agreement with the experimental data than the DSMJ model, while the results of both models converge at large  $n$ .

## 1. Introduction

In the first part of this study [1], hereafter referred to as paper I, we reported new results on measurements of associative ionization (AI) rate constants in collisions between sodium ground-state and Rydberg atoms, obtained in experiments using a single effusive atomic beam. The  $nS$  and  $nD$  Rydberg states with  $n = 8\text{--}20$  were studied. The AI rates were determined by measuring ratios of the molecular  $\text{Na}_2^+$  and the atomic  $\text{Na}^+$  ion signals, whereby the former were created in the AI, while the latter were the product of photoionization of Rydberg states by blackbody radiation (BBR) at room temperature of 300 K. The BBR ionization rates were measured and compared with our new numerical calculations accounting for all possible processes induced by BBR.

The present paper focuses on the theory of collisional ionization of Rydberg atoms. A newly developed stochastic ionization model is used to describe collisions at thermal and sub-thermal energies. We consider ionization in collisions between alkali atoms  $A$  with atoms  $A^{**}$  in Rydberg states:



Reaction (1a) is known as associative ionization (AI). Following Weiner and Boulmer [2], we concisely denote reaction (1b) as Penning-type ionization (PI).

The first detailed theoretical descriptions of the ionization processes (1) were provided by Duman and Shmatov [3], and Mihajlov and Janev [4, 5], whose results are referred to as the DSMJ model. However, the predictions of the DSMJ model often strongly deviate from the experimental data (see, e.g., the reviews by Weiner *et al* [6] and Klucharev [7]).

The present study is an effort to develop a theoretical model allowing a more adequate description of ionizing collisions between ground-state and Rydberg atoms. Our approach involves two essential modifications of the DSMJ model: (i) account for the influence of *twisting effect* [8] on the efficiency of AI channel, and (ii) account for the stochastic dynamics of Rydberg electrons [9–11] during their passage through multiple overlapping level crossings, which are illustrated in figure 1. The effect of collisional  $l$ -mixing, occurring within the hydrogen-like manifold of Rydberg states, is also taken into account. The theory is compared with the experimental data of paper I and of other studies [2, 12, 13].

In what follows, we present the theory for  $\text{Na}^{**}(nl) + \text{Na}$  ionizing collisions, though obtained formulae are valid for other alkali atoms as well. Atomic units  $\hbar = m_e = e = 1$  are used throughout this paper, unless specified otherwise. In section 2 we give an introduction to the existing theories of collisional ionization of Rydberg atoms, and describe some problematic effects disregarded by them. Section 3 introduces the stochastic ionization theory. Section 4 summarizes the formulae used for the present calculations. Section 5 gives the results of calculations and their comparison with the available experimental data.

## 2. Regular dynamics of the Rydberg electron

### 2.1. Nonlinear DSMJ model

The DSMJ model is based on the assumption that the motion of the Rydberg electron is decoupled from the motion of heavy particles. The most important part of ionization dynamics occurs at internuclear distances between 10 and 15 au, which is much smaller than the typical orbit sizes of Rydberg electrons with  $n > 5$ . At such small internuclear separations, the

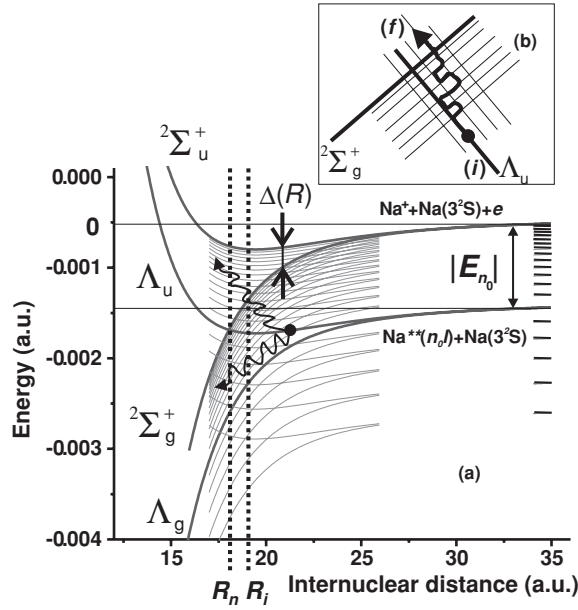


**Figure 1.** Schematic illustration of the mechanism of the  $\text{Na}^{**}(n_0l) + \text{Na}$  collision process. (a) Quasi-molecular potentials involved in the ionization process.  $\Delta(R)$  is the exchange-interaction energy leading to splitting of the potential of  $\text{Na}^+ + \text{Na}$  quasi-molecular ion into the  ${}^2\Sigma_g^+$  and  ${}^2\Sigma_u^+$  states.  $|E_{n_0}|$  is the binding energy of the Rydberg electron in the initial state  $n_0$ . The initial covalent  $\Lambda_u$  state crosses the ionic  ${}^2\Sigma_g^+$  state at  $R = R_n$ , becoming autoionizing for  $R \leq R_n$ . Non-adiabatic transitions (i.e., diffusion of population) to other quasi-molecular states of the Rydberg manifold may increase the distance of the effective crossing point  $R_i$  compared to the initial  $R_n$ . (b) Illustration of Brownian-like migration of the initial population through multiple level crossings of quasi-molecular Rydberg states.

Rydberg electron is literally shared by both nuclei of the quasi-molecular ion  $\text{Na}_2^+$ . Because of charge-exchange interaction between the neutral Na atom and the  $\text{Na}^+$  ion within  $\text{Na}_2^+$ , the inner-shell electron changes its localization from one nucleus to another. In fact, it constitutes a dipole generating a quasi-monochromatic electromagnetic field, which may induce an optical dipole transition of Rydberg electron to the continuum.

Figure 1(a) shows the repulsive  $V_u^+(R)$  and the attractive  $V_g^+(R)$  potentials which correspond to the  ${}^2\Sigma_u^+$  and  ${}^2\Sigma_g^+$  states of  $\text{Na}_2^+$  ion respectively. We calculated these potentials for  $R < 30$  au using the combined valence configuration interaction and the core polarization potential method described in [14]. The potentials of the  $\Lambda_u$  and  $\Lambda_g$  states of the  $\text{Na}_2^{**}$  quasi-molecule are obtained as  $V_u = V_u^+ - |E_n|$  and  $V_g = V_g^+ - |E_n|$ . The exchange interaction term  $\Delta(R)$  is determined as:

$$\Delta(R) = V_u(R) - V_g(R). \quad (2)$$

At large internuclear distances  $R > 30$  au the potentials are well described by asymptotic formulae as [5, 8, 15]

$$V_{u,g}^+(R) = \frac{1}{2} \left[ -\frac{\alpha}{R^4} \pm \Delta(R) \right], \quad (3)$$

$$\Delta(R) = B R^{(2/\gamma)-1} \exp(-\gamma R). \quad (4)$$

Here, the signs '+' and '-' stand for the potentials  $V_u^+$  and  $V_g^+$ , respectively,  $\alpha = 162$  au is the polarizability of Na atoms in the ground state, and  $B = 0.13$  au and  $\gamma = 0.626$  au for Na.

Ionization occurs whenever the frequency of the oscillating dipole  $\omega(R) = \Delta(R)$  exceeds the binding energy  $|E_n|$  of the Rydberg electron. This happens at the critical internuclear distance  $R_n$ , which is defined by the condition

$$\Delta(R_n) = |E_n| = \frac{1}{2n_{\text{eff}}^2} \quad \text{with} \quad n_{\text{eff}} = n - \mu_l, \quad (5)$$

where  $\mu_l$  is the quantum defect for the given  $l$ -series. Note that  $R_n$  corresponds to the crossing point of the incoming covalent curve  $V_u$  and the ionic curve  ${}^2\Sigma_g^+$  (see figure 1(a)). The incoming potential  $V_u$  acquires the autoionization width [4, 5]:

$$W_n(R) = cR^2\omega^3(R)\sigma_{\text{ph}}(\omega(R))/8\pi, \quad (6)$$

where  $\sigma_{\text{ph}}(\omega(R))$  is the photoionization cross-section of the unperturbed Rydberg atom by photons with frequency  $\omega(R)$ , and  $c$  is the speed of light.

The collision process can branch into associative and Penning-type ionization channels (see reaction (1)), depending on the relative kinetic energy  $E = E(R = \infty)$  of the colliding nuclei. The PI and AI processes take place in well-separated regions of internuclear distances, such that

$$\begin{cases} R \geq R_1 \Rightarrow \text{Pening-type-ionization;} \\ R < R_1 \Rightarrow \text{associative ionization,} \end{cases}$$

where  $R_1$  is defined by the condition [2]

$$\Delta(R_1) = E. \quad (7)$$

Hence the region of associatively ionizing internuclear distances is

$$R < R_0, \quad \text{where} \quad \begin{cases} R_0 = R_1, & \text{if } E > |E_n|; \\ R_0 = R_n, & \text{if } E \leq |E_n|. \end{cases} \quad (8)$$

The cross section of the AI process is determined by the probability  $P_{\text{AI}}$  of AI related to an individual trajectory of the colliding pair. For a given initial collision energy  $E$ , the cross section is obtained by integrating the probability over the range of possible impact parameters  $\rho$  [2]:

$$\sigma_{\text{AI}}(E) = 2\pi \int_0^{\rho_{\text{max}}} P_{\text{AI}}(\rho, E) \rho \, d\rho. \quad (9)$$

The probability  $P_{\text{AI}}$ , in turn, depends on the given initial molecular potential  $V_u(R)$  and the distance dependent collision velocity  $v_r(R)$  [4, 2]:

$$P_{\text{AI}}(\rho, E) = \exp\left(-g\theta(R_n - R_1) \int_{R_1}^{R_n} \frac{W(R) \, dR}{v_r(R)}\right) \left[1 - \exp\left(-2g \int_{R_m}^{R_0} \frac{W(R) \, dR}{v_r(R)}\right)\right], \quad (10)$$

$$v_r(R) = \sqrt{\frac{2}{M} \left(E - V_u^+(R) - E \frac{\rho^2}{R^2}\right)}, \quad (11)$$

where  $g = 1/2$  is the statistical factor describing the probability that the colliding system will evolve along the repulsive potential  $V_u$  [2],  $R_m$  is the internuclear distance of turning point of the trajectory, where  $v_r(R_m) = 0$ , the autoionization width  $W(R)$  is given by equation (6), and  $M = 21\,114$  au is the reduced mass of two colliding sodium atoms.

The first multiplier in equation (10) gives the decrease of population in the initial  $nl$  state due to Penning-type ionization within the interval of internuclear distances  $(R_1, R_n)$ .

This results in the presence of the Heaviside function in equation (10), where  $\theta(x \geq 0) = 1$  and  $\theta(x < 0) = 0$ . Noteworthy, this multiplier was missed in [2]. The second multiplier in equation (10) describes the probability of electron emission in the AI region of internuclear distances between  $R_m$  and  $R_0$ . The largest possible impact parameter  $\rho_{\max}$ , for which the AI is still possible, occurs when  $R_0$  coincides with the turning point  $R_m$ , i.e. when  $R_0$  satisfies the equation  $v_r(R_0) = 0$  [2]:

$$\rho_{\max} = \rho(R_m = R_0) \quad \text{where} \quad \rho(R_m) = R_m \sqrt{1 - \frac{V_u^+(R_m)}{E}}. \quad (12)$$

## 2.2. Rate constants and velocity distributions

The ionization rate constant, which is directly measured in experiments, results from averaging the cross-section over the collision energy distribution  $f(E)$

$$k_{\text{AI}} = \int_{E_{\min}}^{\infty} \sigma_{\text{AI}}(E) \left(\frac{2E}{M}\right)^{1/2} f(E) dE. \quad (13)$$

In order to compare theory with experimental data, the theoretical cross sections must be averaged according to equation (13) over the particular distribution of collision velocities  $v_c = \sqrt{2E/M}$  of each individual experiment. In a gas cell at temperature  $T_{\text{gc}}$  this distribution is given by the Maxwell function

$$F_{\text{Maxwell}}(v_c) = \sqrt{\frac{2}{\pi}} \left(\frac{M}{T_{\text{gc}}}\right)^{3/2} v_c^2 \exp\left(-\frac{Mv_c^2}{2T_{\text{gc}}}\right). \quad (14)$$

Here and in the equations below the temperatures are in energy atomic units. A somewhat similar distribution was obtained for two effusive atomic beams crossed at right angles [6, 16]:

$$F_{\text{cb}}(v_c) = v_c^5 \left(\frac{M}{T_{\text{bs}}}\right)^3 \exp\left(-\frac{Mv_c^2}{T_{\text{bs}}}\right). \quad (15)$$

The distribution becomes dramatically different from both previous ones for collisions within a single effusive beam [16]:

$$F_{\text{sb}}(v_c) \cong \frac{2.96}{\sqrt{2\pi M T_{\text{bs}}}} \frac{M}{\sqrt{1 + 9\pi M v_c^2 / 128 T_{\text{bs}}}} \exp\left(-\frac{Mv_c^2}{T_{\text{bs}}}\right). \quad (16)$$

In equations (15) and (16) the parameter  $T_{\text{bs}}$  is the temperature of the effusive beam source, whereby in equation (15) it is assumed that both sources are kept at the same temperature.

## 2.3. Twisting effect

The lower limit of integral (13) is determined by the minimal collision energy  $E_{\min}$  required to reach the critical distance  $R_0$  [2] (see also equation (12))

$$E_{\min} = \max[V_u(R_0) + |E_n|, 0]. \quad (17)$$

One can easily find that  $E_{\min} = 0$  for Rydberg states of sodium with  $n_{\text{eff}} > 14$ . This means that energy threshold of ionization vanishes for these states. In that case, even very low-energy collisions can efficiently lead to ionization. However, ionization may be hindered by *twisting* of the colliding pair in the attractive potential [8], which was disregarded by the DSMJ model.

The crossing point  $R_n$  of the covalent and ionic curves can only be reached if the turning point of the given trajectory is  $R_m < R_n$ . This is valid for impact parameters  $\rho < \rho_{\max}(R_n)$ ,

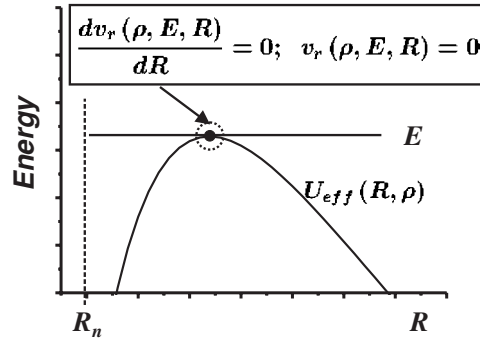


**Figure 2.** Passage of the  $\text{Na}^{**} + \text{Na}$  colliding system over the potential barrier of the effective potential  $U_{\text{eff}}$ , created by centrifugal forces. The barrier limits the range of impact parameters that can bring atoms  $\text{Na}^{**}$  and  $\text{Na}$  to distances as small as  $R_n$ .

where  $\rho_{\text{max}}$  is given by equation (12). The collisional ionization cross section at low energies can be estimated as

$$\sigma_i(E) \sim \pi \rho_{\text{max}}^2 \sim 1/E. \quad (18)$$

For the velocity distribution (16), the integrand in equation (13) is proportional to  $1/E$ , and the integral diverges for  $n_{\text{eff}} > 14$ , because integration starts from  $E = 0$ . To avoid the divergence, one must consider an additional potential barrier caused by centrifugal part of the effective potential at large internuclear distances (figure 2). The radial velocity of colliding atoms in the long-range polarization potential  $V_u(R) + |E_n| \approx -\alpha/(2R^4)$  is

$$v_r = \sqrt{\frac{2}{M} \left( E + \frac{\alpha}{2R^4} - E \frac{\rho^2}{R^2} \right)}. \quad (19)$$

For sufficiently large impact parameters this velocity becomes imaginary for  $R < R_n$ . In other words, the colliding atoms cannot overcome the potential barrier built by centrifugal forces at large internuclear distances. At small impact parameters, in contrast, the atoms easily pass over the (lower in this case) barrier. For a given collision energy  $E$ , there exists a critical value of impact parameter  $\rho = \rho_{\text{twist}}$ , at which the radial velocity of the colliding atoms turns to zero on the top of the effective potential  $U_{\text{eff}}(R) = -\alpha/2R^4 + E\rho^2/R^2$  (see figure 2). This corresponds to mutual twisting of atoms of the colliding pair [8]. The critical impact parameter can be obtained from the equation system:

$$\begin{cases} v_r(\rho, E, R) = 0; \\ \frac{\partial v_r(\rho, E, R)}{\partial R} = 0. \end{cases} \quad (20)$$

The solution of equations (20) yields

$$\rho_{\text{twist}} = (2\alpha/E^{1/4}). \quad (21)$$

This value puts an additional constraint on the trajectories leading to associative ionization, besides condition (12). The final value, which must be used as an upper integration limit in calculation of the AI cross section, is the smallest of those given by equations (12) and (21):

$$\tilde{\rho}_{\text{max}} = \min[\rho_{\text{max}}(R_0), \rho_{\text{twist}}]. \quad (22)$$

If  $\rho > \tilde{\rho}_{\text{max}}$ , the distance  $R_n$  (or  $R_0$ ) cannot be reached, and ionization (or AI) does not occur. Importantly, condition (22) removes the divergence of integral (13), because at low energies  $\sigma(E) \sim \pi \rho_{\text{twist}}^2 \sim 1/\sqrt{E}$ , in contrast to the  $1/E$  dependence of equation (18).

### 3. Stochastic dynamics of the Rydberg electron

The oscillating dipole electric field, produced by exchange interaction within the  $\text{Na}_2^+$  ion, causes strong coupling of the Rydberg electron to the internal dipole of the ionic core of the quasi-molecule [2, 17]. This strong coupling has two important consequences: (i) the first-order (linear) approximation of interaction of the Rydberg electron with the core breaks down [2]; (ii) efficient Landau–Zener-like transitions may occur in the region of multiple crossings of the molecular Rydberg states (see figure 1(b)). The latter implies that the meaning of threshold distance  $R_n$  is somewhat diffuse. Non-adiabatic transitions at multiple level crossings lead to change of the effective threshold distance  $R_i$  of ionization (figure 1), which can be larger than the threshold  $R_n$ . It is a non-trivial task, however, to account for multiple and in part overlapping level crossings, because the conventional Landau–Zener approximation assumes that all crossings are well isolated from each other. For Rydberg states with high densities of energy levels such an assumption is not valid.

#### 3.1. Diffusion equation

An alternative approach in modelling multiple level crossings was proposed in [9–11], where the concept of dynamic chaos [18, 19] was applied to the Rydberg-electron dynamics. One can describe the migration of the colliding system through the net of Rydberg states as diffusion of the electron in the space of its effective quantum numbers  $n_{\text{eff}}$  [20–22]. Slow collisions assume the validity of the adiabatic approximation, which is true for  $n < 25$  at thermal collision velocities [23]. In that case, the theory developed to describe the stochastic drift of a Coulomb electron in a microwave field [20, 22, 24] can be used to describe the population distribution  $f(n_{\text{eff}}, t)$  within the region  $\Omega_{\text{chaos}}$  in the  $n_{\text{eff}}$  space, where the motion of the Rydberg electron is chaotic. This can be done by using a Fokker–Planck-type equation, as suggested in [9]:

$$\frac{\partial}{\partial t} f(n_{\text{eff}}, t) = \frac{\partial}{\partial n_{\text{eff}}} j. \quad (23)$$

Here,  $j$  is the diffusion flux,

$$j = D(n_{\text{eff}}, R) \frac{\partial f(n_{\text{eff}}, t)}{\partial n_{\text{eff}}}, \quad (24)$$

and  $D$  is the diffusion coefficient,

$$D(n_{\text{eff}}, R) = n_{\text{eff}}^3 \tilde{D}(R); \quad \tilde{D}(R) = 0.023 R^2 \Delta^{8/3}(R) [1 + 1.18 \Delta^{2/3}(R) L^2]. \quad (25)$$

The parameter  $L = (l + 1/2)$  in equation (25) specifies the semi-classical orbital momentum [23], and it varies on a time scale which is much longer than the diffusion time  $\tau_{\text{dif}}$  of electron in the  $n_{\text{eff}}$  space [25].

The adiabatic approximation, which is used in the present treatment, assumes that electronic motion adiabatically adjusts to the comparatively slow variation of the nuclear configuration in the course of the collision. The slow variation of internuclear distance  $R = R(t)$  with time implies that the diffusion coefficient (25) is a time-dependent variable of equation (23). The time dependence of  $R(t)$  may be determined in the same way as in the DSMJ model, i.e., by considering the motion of nuclei along the repulsive potential  $V_u^+(R)$ .

In fact, the reduced diffusion coefficient  $\tilde{D}(R)$  in equation (25) corresponds to the case of a Coulomb-like electron, ignoring the real potential of the atomic core  $A^+$ . This imperfection was overcome in [10] using a single-channel quantum-defect method. The authors analysed the motion of the perturbed Rydberg electron within the diatomic complex  $AA^{**}$ . Using the

Kepler map technique [26], the reduced diffusion coefficient in equation (25) was determined as

$$\tilde{D}(R) = \frac{\omega^4 R^2}{48\pi} \sum_{\Delta l = \pm 1} L_c^4 D_{\Delta l}^2(\omega), \quad (26)$$

where  $\omega = \Delta(R)$ ,  $L_c = (l + 1/2 + \Delta l/2)$ , and

$$D_{\Delta l}(\omega) = \left[ -\frac{\sin(\pi \Delta \mu)}{2} - \frac{\sqrt{\pi}}{x} \Phi'_{\Delta \mu}(x) + \Delta l \sqrt{\frac{\pi}{x}} \Phi_{\Delta \mu}(x) \right], \quad (27)$$

with  $x = (\omega L_c^3/2)^{2/3}$ . Functions  $\Phi$  and  $\Phi'$  relate to the Airy function:

$$\Phi_{\Delta \mu}(x) = \frac{1}{\sqrt{\pi}} \int_0^\infty \cos(x\xi + \xi^3/3 + \pi \Delta \mu) d\xi, \quad \Phi'_{\Delta \mu}(x) = \frac{d}{dx} \Phi_{\Delta \mu}(x). \quad (28)$$

The summation over  $\Delta l$  in equation (26) takes into account the dipole transitions between Rydberg orbits that change the orbital quantum number  $l$  by  $\pm 1$ . For  $nS$  states the term with  $\Delta l = -1$  in equation (26) must be dropped.

Equations (26) and (27) were obtained by analysing the semi-classical representations [27] of the dipole matrix element  $\langle nl|r|n'l' \rangle$  of bound-bound transitions with  $E_{n'} = (E_n \pm \omega)$ , where  $\omega = \Delta(R)$  is the exchange frequency. The factor  $\Delta \mu = \mu_{l+\Delta l} - \mu_l$  gives the quantum defect difference between Rydberg series with  $l$  and  $l' = l + \Delta l$ . In the case of hydrogen-like levels with small quantum defect and small value of the parameter  $x$ , which is a common situation for transitions between Rydberg levels, equation (26) for  $\tilde{D}(R)$  reduces to the representation of equation (25). Besides the bound-bound transitions, the autoionization width (6) can also be written in an explicit form using the semi-classical formulae of [27] for photoionization cross-section:

$$W_n(R) = \tilde{W}(R)/n_{\text{eff}}^3; \quad (29)$$

$$\tilde{W}(R) = \frac{\omega^2 R^2}{12\pi} \sum_{\Delta l = \pm 1} \frac{L_c^5}{l + 0.5} D_{\Delta l}^2(\omega). \quad (30)$$

The accuracy of these equations was estimated to be better than 10% [11, 27].

### 3.2. Boundary conditions

For a given (and not too large) internuclear distance, three characteristic regions in the  $n_{\text{eff}}$  space of Rydberg electron can be distinguished (see figure 3). The standard mapping [18, 19, 26] and the Chirikov criterion [25] allow the determination of the zone  $\Omega_{\text{chaos}}$  of multiple level crossings in the range  $N_{\text{chaos}}(R) < n_{\text{eff}} < N_{\text{auto}}(R)$ , within which the Rydberg electron undergoes chaotic motion. The  $R$ -dependent quantum number  $N_{\text{chaos}}(R)$  is implied by the technique of standard (Kepler) mapping [10]:

$$N_{\text{chaos}}^5(R) = \frac{1}{12\pi\omega\sqrt{2\pi\tilde{D}(R)}}, \quad (31)$$

such that the diffusion flux  $j(n_{\text{eff}} = N_{\text{chaos}}) = 0$ . The number  $N_{\text{chaos}}(R)$  restricts the random motion of Rydberg electron to states with sufficiently large  $n_{\text{eff}}$ . The states with  $n_{\text{eff}} < N_{\text{chaos}}(R)$  define the zone  $\Omega_{\text{reg}}$ , which corresponds to regular motion of the Rydberg electron. The diffusion is not possible inside  $\Omega_{\text{reg}}$  because of too large energy separation between the neighbouring levels, which ensures that the dynamic resonances do not overlap. This means that in the process of diffusive migration within the zone  $\Omega_{\text{chaos}}$  the Rydberg

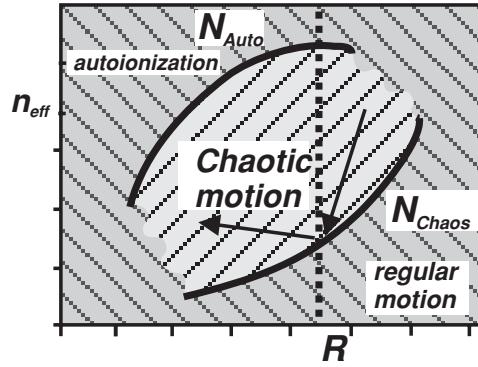


**Figure 3.** Illustration of boundary conditions of the diffusion equation (23). The curve  $N_{\text{chaos}}(R)$  (see equation (31)) separates the zones  $\Omega_{\text{chaos}}$  and  $\Omega_{\text{reg}}$  of chaotic and regular motion of Rydberg electron. The curve  $N_{\text{auto}}(R)$  (see equation (32)) separates the chaotic motion zone  $\Omega_{\text{chaos}}$  from the zone  $\Omega_{\text{ion}}$ , within which Rydberg electron is in an autoionizing state.

electron cannot penetrate into the zone  $\Omega_{\text{reg}}$ . The point  $N_{\text{chaos}}(R)$  is thus playing the role of a reflecting boundary, at which the diffusion flux  $j$  (see equation (24)) turns to zero. Importantly, the position of the reflection point varies with  $R = R(t)$ , making the boundary condition (31) time dependent.

The third zone  $\Omega_{\text{ion}}$  corresponds to Rydberg levels with  $n_{\text{eff}} > N_{\text{auto}}(R)$ . Within this zone Rydberg electrons can be ionized by the internal electric dipole field. Quantum transitions to the continuum at a given  $R$  are possible when  $\omega(R) = \Delta(R) > 1/2n_{\text{eff}}^2$ , i.e.,

$$n_{\text{eff}} > N_{\text{auto}}(R) = \frac{1}{\sqrt{2\omega(R)}}. \quad (32)$$

Since there are no crossings in the autoionization zone  $\Omega_{\text{ion}}$  (see figure 1), no population diffusion occurs. Instead, as soon as the Rydberg electron migrates beyond  $n = N_{\text{auto}}(R)$ , the Rydberg  $n$ -level begins to ionize at the rate  $W(R)$ , equation (29), which is determined by the autoionization width of the DSMJ model given by equation (6). In fact, there are some additional boundary conditions at  $N_{\text{auto}}(R)$ , related to the continuity of  $f(n_{\text{eff}})$  and  $j(n_{\text{eff}})$  with vanishing  $f(n_{\text{eff}} = \infty)$ , which are described in [11] and which we do not discuss here for the sake of conciseness.

#### 4. Analytical formulae for ionization rates

A numerical algorithm allowing the solution of equation (23) and thus the determination of the reaction cross section  $\sigma(E)$  according to equation (9) was reported in [9]. An alternative analytical method for the evaluation of  $\sigma(E)$ , with a typical accuracy of 15%, was described in [9, 10]. In this section, we briefly outline further development of analytical approaches allowing the discrimination between the associative and Penning type ionization channels of reaction (1).

##### 4.1. Effective collision and diffusion times

The semi-classical representation of the diffusion coefficient, equations (25) and (26), and the resulting structure of the master equation (23), allow the reduction of the latter to a standard steady-state form. Indeed, one can divide both sides of equation (23) by  $\tilde{D}(R)$  and introduce

the effective time  $\tilde{t}(R)$ , such that  $d\tilde{t} = dt \tilde{D}(R)$ , during which the nuclei reach the internuclear distance  $R$ . With such modification, equation (23) within the stochastic zone  $\Omega_{\text{chaos}}$  can be rewritten in the form

$$\frac{\partial}{\partial \tilde{t}} f(n_{\text{eff}}, \tilde{t}) = \frac{\partial}{\partial n_{\text{eff}}} D_{\text{stat}}(n_{\text{eff}}) \frac{\partial}{\partial n_{\text{eff}}} f(n_{\text{eff}}, \tilde{t}), \quad (33)$$

where  $D_{\text{stat}}(n_{\text{eff}}) = n_{\text{eff}}^3$  is the stationary diffusion coefficient, which has a form typical of the theory of Rydberg electron migration in a microwave electric field [25, 26].

The effective time  $\tilde{t}(t) = \tilde{t}(R(t))$  is a function of the internuclear distance  $R$ ,

$$\tilde{t}(R) = \int_R^\infty \frac{dR_{\rho,E}^{(u)}}{v_r(R_{\rho,E}^{(u)})} \tilde{D}(R_{\rho,E}^{(u)}) \theta(n_{\text{eff},0} - N_{\text{chaos}}(R_{\rho,E}^{(u)})), \quad (34)$$

where indices  $\rho, E$  and  $(u)$  in the integrand emphasize that the effective time is defined along the classical trajectory  $R_{\rho,E}^{(u)}(t)$  of the nuclei moving on the potential  $V_u$ , the radial velocity  $v_r$  is given by equation (11), and  $n_{\text{eff},0}$  is the effective quantum number of the initially excited Rydberg level. Note that the effective time  $\tilde{t}$  has finite values, because  $\tilde{D}(R)$  decreases rapidly with increasing  $R$ , and the initial level  $n_{\text{eff},0}$  lies outside the stochastic zone  $\Omega_{\text{chaos}}$  at large internuclear distances.

Equations (33) and (34) allow the following interpretation of the collision process after atoms have been selectively prepared in the state  $n_{\text{eff},0}$ . As the atoms approach each other, the level  $n_{\text{eff},0}$  enters the  $\Omega_{\text{chaos}}$  zone, and population begins to diffuse towards other levels  $n_{\text{eff}}$  within this zone. It takes time  $\tilde{t}(R)$  for the atoms to arrive at internuclear distance  $R$ , and this time gives the time interval for the diffusion equation (33). Of interest is only the first half of the collision, during which the colliding  $\text{Na}^{**}(nl) + \text{Na}$  system moves towards the ionic potential  $^2\Sigma_g^+$  (see figure 1).

In fact, it is possible to introduce an accurate measure of the effective diffusion time,  $\tau_{\text{diff}}(R)$ , which gives the mean time needed for the Rydberg electron to migrate from the initial state  $n_{\text{eff},0}$  to the autoionization boundary  $N_{\text{auto}}(R)$  given by equation (32). Several approaches to the evaluation of  $\tau_{\text{diff}}(R)$  have been proposed (see, e.g., [28]). The authors of [9] suggest replacing  $\tau_{\text{diff}}(R)$  with the *mean first passage time*, which is defined as [29]:

$$\tau_{\text{MFPT}}(n_{\text{eff},0}) = \int_0^\infty d\tilde{t} \int_{N_{\text{chaos}}}^{N_{\text{auto}}} f(n_{\text{eff}}, \tilde{t}) dn_{\text{eff}}, \quad (35)$$

where the distribution function  $f(n_{\text{eff}}, \tilde{t})$  depends on  $n_{\text{eff},0}$  via the initial condition  $f(n_{\text{eff}}, \tilde{t} = 0) = \delta(n_{\text{eff}} - n_{\text{eff},0})$ . The function  $\tau_{\text{MFPT}}(n_{\text{eff},0})$  possesses a remarkable property that it satisfies the following simple steady-state equation [9]:

$$-1 = \frac{\partial}{\partial n_{\text{eff},0}} D_{\text{stat}}(n_{\text{eff},0}) \frac{\partial}{\partial n_{\text{eff},0}} \tau_{\text{MFPT}}(n_{\text{eff},0}), \quad (36)$$

which yields

$$\tau_{\text{MFPT}}(n_{\text{eff},0}) = \int_{n_{\text{eff},0}}^{N_{\text{auto}}} dn_{\text{eff}} \frac{n_{\text{eff}} - N_{\text{chaos}}}{D_{\text{stat}}(n_{\text{eff}})}. \quad (37)$$

Equation (37) is a solution of equation (35) at  $\tau_{\text{MFPT}}(n_{\text{eff},0} = N_{\text{auto}}) = 0$  and  $\partial \tau_{\text{MFPT}}(n_{\text{eff},0} = N_{\text{chaos}}) / \partial n_{\text{eff},0} = 0$ . The first requirement implies that no time is needed to reach  $N_{\text{auto}}$  if the initial state coincides with  $N_{\text{auto}}$ . The second requirement results from the boundary condition  $j(n_{\text{eff}} = N_{\text{chaos}}) = 0$ .

The use of  $\tau_{\text{MFPT}}(n_{\text{eff},0})$  instead of  $\tau_{\text{diff}}(R)$  is valid only near the boundary  $N_{\text{chaos}}$  [9, 30]. Therefore, the authors of [30], after solving a number of model problems, recommended to

modify  $\tau_{\text{MFPT}}(n_{\text{eff}}, 0)$  and use for  $\tau_{\text{diff}}(R)$  the value

$$\tau_{\text{diff}}(R) = 4.5\tau_{\text{MFPT}}(n_{\text{eff},0}) \quad \text{with} \quad \tau_{\text{MFPT}} = \int_{n_{\text{eff},0}}^{N_{\text{auto}}} dn_{\text{eff}} \frac{n_{\text{eff}} - n_{\text{eff},0}}{D_{\text{stat}}(n_{\text{eff}})}. \quad (38)$$

The multiplier 4.5 was found from explicit solution of a reference problem, modelling diffusion processes in a half-space. Using the function  $D_{\text{stat}}(n_{\text{eff}}) = n_{\text{eff}}^3$  as in equation (33), equation (38) can be rewritten in an explicit form

$$\tau_{\text{diff}}(R) = 4.5 \frac{(n_{\text{eff},0} - N_{\text{auto}}(R))^2}{2n_{\text{eff},0}N_{\text{auto}}^2(R)}. \quad (39)$$

#### 4.2. Evaluation of the AI cross sections

The above results allow the determination of both the AI cross sections  $\sigma_{\text{AI}}(E)$  and the total ionization cross sections  $\sigma_i(E)$  through generalization of the method proposed in [9, 10] for calculation of  $\sigma_i(E)$ . The key step is the comparison of the effective time  $\tilde{\tau}(R)$  of motion along each specific trajectory  $R_{\rho,E}^{(u)}(t)$  with the time  $\tau_{\text{diff}}(R)$ , in which the autoionization boundary  $N_{\text{auto}}(R)$  is reached. If  $\tilde{\tau}(R) > \tau_{\text{diff}}(R)$ , the collision time is sufficiently long to allow the population to diffuse and reach the autoionization boundary  $N_{\text{auto}}(R_i)$  at the distance  $R_i(\rho, E)$  (see figure 1), which happens at time  $\tilde{\tau}_i < \tilde{\tau}$ . The point  $R_i$  satisfies the equation

$$\tilde{\tau}(R_i) = \tau_{\text{diff}}(R_i), \quad (40)$$

whereby the population has diffused from the initial state  $n_{\text{eff},0}$  to the state

$$n_{\text{eff},i}(\rho, E) = N_{\text{auto}}(R_i). \quad (41)$$

As soon as the crossing point of the ionic potential  ${}^2\Sigma_g^+$  with the potential  $V_u$  associated with the  $n_{\text{eff},i}(\rho, E)$  state has been reached at  $R = R_i$ , the Rydberg electron stabilizes its location in the energy space at  $n_{\text{eff},i}$ . The probability of AI reaction and its cross section can now be found by using the results of DSMJ model, equations (9), (10), and by replacing the crossing point  $R_n$ , corresponding to the initial effective quantum number  $n_{\text{eff},0}$ , with  $R_i(\rho, E)$ , corresponding to  $n_{\text{eff},i}(\rho, E)$ .

If for a given trajectory  $R_{\rho,E}^{(u)}(t)$  the effective time  $\tilde{\tau}(R)$  is less than  $\tau_{\text{diff}}(R)$  for all  $R$ , the Rydberg electron has a vanishing probability of reaching the autoionization limit, and the collision with such an impact parameter  $\rho$  does not contribute to the ionization. This assumption dates back to the studies of Weisskopf [31], and it works well for the evaluation of the total cross section [9]. The critical value  $\rho_{\text{crit}}$  of impact parameter, defining the range of impact parameters  $\rho \leq \rho_{\text{crit}}$ , which can potentially lead to ionization, can be determined by setting  $R_i$  as the turning point of the trajectory  $R_{\rho_{\text{crit}},E}^{(u)}(t)$  [9]. Note that if  $R_i > R_n$ , the critical impact parameter  $\rho_{\text{crit}} > \rho_{\text{max}}$  (cf equation (12)), i.e., the diffusion can extend the range of associatively ionizing impact parameters beyond those presumed by the DSMJ model. The limitation  $\rho < \rho_{\text{twist}}$  imposed by the twisting effect (equation (21)) remains valid also in the case of diffusion.

#### 4.3. Accuracy and limitations

Both DSMJ and stochastic models use the adiabatic approximation and classical description of motion of the colliding nuclei. The de Broglie wavelength of an atom in an effusive beam at the source temperature of  $T_{\text{bs}} = 600$  K is  $\lambda_{\text{db}} = 2\pi/\sqrt{2mT_{\text{bs}}} = 0.5$  au, where  $m = 42\,228$  au is the mass of the Na atom. This is much smaller than the characteristic distances  $R_i = 10\text{--}15$  au, at which the diffusion and ionization processes typically occur.

Hence, the classical consideration of nuclear trajectories is a valid approach. The adiabatic approximation, however, is applicable only within a limited range of the effective quantum numbers  $n_{\text{eff}}$ , which is imposed by the following conditions [8, 23]:

(i) the average relative velocities  $\langle v_c \rangle$  of the colliding nuclei must be small compared to the mean square velocity of the Rydberg electron  $\langle v_n \rangle = 1/n_{\text{eff}}$ . In the case of the single beam experiment [1], in which  $\langle v_c \rangle = 360 \text{ m s}^{-1} = 1.6 \times 10^{-4} \text{ au}$ , it is fulfilled for states with  $n_{\text{eff}} \ll 6000$ ;

(ii) the Massey parameter  $\xi$  must be sufficiently large:

$$\xi = \frac{\Delta E_n R_i}{\langle v_c \rangle} > 1.$$

Here  $\Delta E_n \sim n_{\text{eff}}^{-3}$  is the energy separation between neighbouring Rydberg levels. Under the conditions of present study  $R_i \sim 10\text{--}15 \text{ au}$ . Hence, the Massey criterion is fulfilled for  $n_{\text{eff}} < 36$ ;

(iii) in our model we work in the approximation of a common trajectory [8] for the internuclear motion, i.e., we assume that the relative kinetic energy  $E$  of the colliding pair exceeds the energy separation between adjacent Rydberg states on the energy level diagram of figure 1:  $E > \Delta E_n \sim n_{\text{eff}}^{-3}$ . In crossed beams of two sources at the temperature of  $T_{\text{bs}} = 600 \text{ K}$  the mean collision energy is  $E = 0.0026 \text{ au}$ , which requires that  $n_{\text{eff}} > 7$ . Under the single-beam conditions the mean collision velocity is three times smaller than in crossed beams [16], which results in the reduction of relative kinetic energy by a factor of 9. Therefore, in the single-beam case of paper I the stochastic model is strictly valid only for  $n_{\text{eff}} > 15$ . The consequences of this requirement are discussed in sections 5.3.

Beginning from about  $n_{\text{eff}} = 25$ , the *shake-up mechanism* gives a noticeable contribution to the ionization [23, 32]. This mechanism is related to the change of localization of inner shell electron between the two nuclei, which is seen by the Rydberg electron as a sudden change of the velocity of the effective Coulomb centre. In the present study we consider Rydberg states with  $n_{\text{eff}} < 25$ , for which the adiabatic approximation is valid at thermal collision energies [23]. Note that the Chirikov criterion presumes overlap of the neighbouring Landau–Zener crossing points in figure 1(b). Such overlap leads to strong dephasing of different Landau–Zener trajectories connecting the initial and final states in figure 1(b). As was shown in [18], under such conditions it is reasonable to apply the quantum-kinetics technique [33]. Although we use in calculations the diffusion coefficient in the form (25) and (26), obtained in [10] using the classical approach of the stochastic dynamics, the semi-classical result of equation (26) for  $\tilde{D}(R)$  turns out to be identical with that obtained by quantum kinetics (see also [28]).

## 5. Results and discussion

Comparison between the experimental data and the theoretical predictions requires detailed analysis of the conditions of each experiment. It is necessary to take into account any possible secondary and background processes, as such may significantly influence the apparent ionization rates measured in experiments. In this section we examine the effects of collisional  $l$ -mixing, and BBR-induced and spontaneous mixing of Rydberg states. Finally, we compare our theory with the available experimental data.

### 5.1. Effect of $l$ -mixing

For  $nl$  states of alkali atoms with  $l \geq 2$ , the cross sections of  $\text{Na}^{**}(nl) + \text{Na} \rightarrow \text{Na}^{**}(n'l) + \text{Na}$  collisional  $l$ -mixing are known [32, 34] to be close to geometrical cross sections of Rydberg

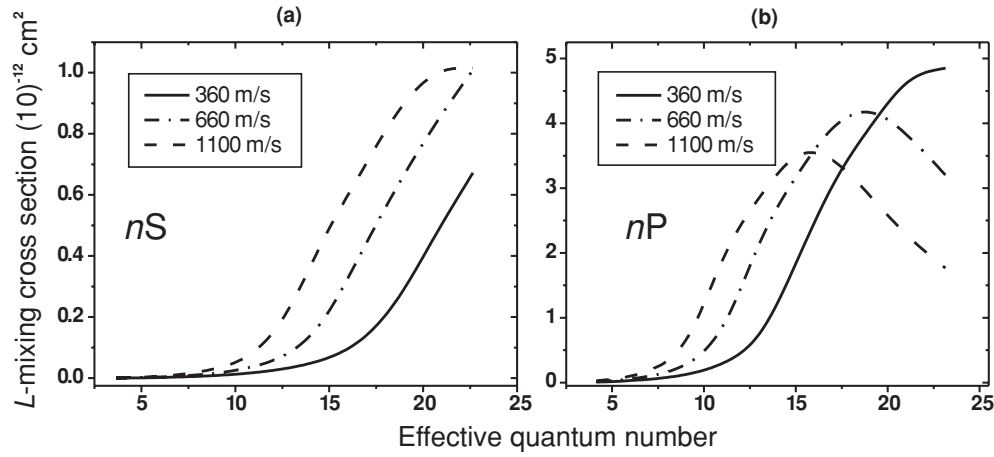


**Figure 4.**  $l$ -mixing cross-sections of (a)  $nS$  and (b)  $nP$  states of Na at mean collision velocities of  $360 \text{ m s}^{-1}$ ,  $660 \text{ m s}^{-1}$  and  $1100 \text{ m s}^{-1}$ .

atoms [35]:

$$\sigma_{\text{geom}} = \pi \langle r^2 \rangle \frac{1}{2l+1} \sum_{m=-l}^{m=l} \frac{|m|}{\sqrt{l(l+1)}} = \pi \frac{n^2}{2} [5n^2 + 1 - 3l(l+1)] \frac{\sqrt{l(l+1)}}{2l+1}. \quad (42)$$

The summing is performed over  $(2l+1)$  possible spatial orientations of the Rydberg orbit.

Figure 4 shows the results of calculations of  $l$ -mixing cross sections  $\sigma_{\text{mix}}(E)$  for  $nS$  and  $nP$  states of Na using the formulae of [23, 32]. Comparison of the data in figure 4 with equation (42) shows that for Na( $nS$ ) states the mixing parameter is  $\Lambda = \sigma_{\text{mix}}(E)/\sigma_{\text{geom}} < 0.06$ . For the  $nP$  states, the mixing is stronger, e.g., for the Na<sup>\*\*</sup>(12P) state  $\Lambda = 0.9, 0.6$  and  $0.2$  for collision velocities of  $1100 \text{ m s}^{-1}$ ,  $660 \text{ m s}^{-1}$  and  $360 \text{ m s}^{-1}$ , respectively. Such strong dependence on collision velocity arises due to the energy gap between the  $nP$  state and the other states of the hydrogen-like  $n$ -manifold, which is involved in the  $l$ -mixing process.

The processes of  $l$ -mixing typically proceed at large internuclear distances  $R_{\text{mix}} \approx \langle r \rangle_n = 3n_{\text{eff}}^2/2 \text{ au}$ . This is much larger than the typical distances of ionization,  $R_i \sim R_n \sim (10-15) \text{ au}$ . During the collision, the initially excited  $|n, l\rangle$  level is converted into a superposition of partial waves  $|n, l'\rangle$  at  $R \sim R_{\text{mix}}$ , before the colliding atoms reach the ionization distance  $R_i$ . Since the stochastic processes leading to ionization proceed at sufficiently low rates, they do not cause any further  $l$ -mixing [25], so that each partial wave  $|n, l'\rangle$  evolves independently and contributes to the ionization rate (13) according to its statistical weight. Therefore, in the case of a complete  $l$ -mixing (i.e. for  $\Lambda = 1$ ) the total rate constant should be calculated by summing the contributions  $k_{\text{AI}}(n, l')$  of individual  $l'$ -states with the statistical weights  $\frac{1}{n^2}(2l'+1)$ :

$$k_{\text{AI}}^{\text{mix}}(n) = \frac{1}{n^2} \sum_{l'=0}^{n-1} (2l'+1) k_{\text{AI}}(n, l'). \quad (43)$$

In the below calculations we assume a complete  $l$ -mixing for  $nD$  and  $nP$  states and no mixing for  $nS$  states.

### 5.2. Population redistribution due to spontaneous and BBR-induced transitions

As has been shown in paper I, blackbody radiation (BBR) and spontaneous decay lead to redistribution of population of the initially excited  $nI$  Rydberg state over a wide range of other  $n'I'$  states. This effect is especially important for the  $nS$  and  $nD$  states due to their relatively short lifetimes. Suppose a single  $nS$  state is excited. After the excitation, spontaneous and BBR-induced processes lead to an appreciable population of the  $n'P$  states (see figure 5 in paper I). The total formation rate of  $\text{Na}_2^+$  ions is thus composed of contributions due to AI in collisions with atoms in the  $nS$  state and with atoms in various  $n'P$  states:

$$\frac{dN_{\text{Na}_2^+}(t)}{dt} = k_{\text{AI}}^{nS} N_{nS}(t) n_{3S} + \sum_{n'} k_{\text{AI}}^{n'P} N_{n'P}(t) n_{3S}, \quad (44)$$

where  $n_{3S}$  is the number density of atoms in the ground state,  $N_{\text{Na}_2^+}(t)$  is the number of the molecular ions produced per time unit in the AI, and  $k_{\text{AI}}^{nS}$  and  $k_{\text{AI}}^{n'P}$  are the AI rate constants for  $nS$  and  $n'P$  states, respectively.

The total number of atoms in the  $nS$  state,  $N_{nS}(t)$ , decreases with a time constant determined by the effective lifetime  $\tau_{\text{eff}}^{nS}$  of this state at the ambient temperature of the given experiment:

$$N_{nS}(t) = N_{nS}(0) \exp(-t/\tau_{\text{eff}}^{nS}). \quad (45)$$

Evolution of the population of  $n'P$  levels is described by the rate equation

$$\frac{dN_{n'P}(t)}{dt} = W(nS \rightarrow n'P) N_{nS}(t) - N_{n'P}(t) \tau_{\text{eff}}^{n'P}, \quad (46)$$

where  $W(nS \rightarrow n'P)$  is the rate of population of the  $n'P$  state due to spontaneous and BBR-induced transitions from the  $nS$  state, and  $\tau_{\text{eff}}^{n'P}$  is the effective lifetime of the  $n'P$  state (at 300 K in the case of paper I).

In the experiments [1, 2] the ions were registered during the time interval  $(t_1, t_2)$  after application of a short exciting laser pulse at  $t = 0$ . Integration of equation (44) yields the total number of molecular ions produced during the time interval of ion detection. The result can be written in the form

$$N_{\text{Na}_2^+}|_{t_1}^{t_2} = k_{\text{eff}}^{nS} n_{3S} N_{nS}(0) t_{\text{eff}}^{nS}. \quad (47)$$

In experiments, the effective AI rate constant  $k_{\text{eff}}^{nS}$  is determined. It is defined as

$$k_{\text{eff}}^{nS} = k_{\text{AI}}^{nS} + k_{\text{mix}}^{nS} = k_{\text{AI}}^{nS} + \sum_{n'} \frac{W(nS \rightarrow n'P) k_{\text{AI}}^{n'P}}{1/\tau_{\text{eff}}^{n'P} - 1/\tau_{\text{eff}}^{nS}} \left(1 - \frac{t_{\text{eff}}^{n'P}}{t_{\text{eff}}^{nS}}\right), \quad (48)$$

where the effective interaction time for atoms in the  $nS$  and  $n'P$  states is given by [1]

$$t_{\text{eff}}^{nS, n'P} = \tau_{\text{eff}}^{nS, n'P} [\exp(-t_1/\tau_{\text{eff}}^{nS, n'P}) - \exp(-t_2/\tau_{\text{eff}}^{nS, n'P})]. \quad (49)$$

The main contribution to the sum in equation (48) is due to the  $n'P$  states with  $n' = (n \pm 1)$ . The effective AI rates  $k_{\text{eff}}^{nD}$  for  $nD$  states are determined in the same way, taking into account the BBR-induced transfer to the  $n'P$  and  $n'F$  states.

### 5.3. Comparison of experimental data with the theory for $nS$ , $nP$ and $nD$ states of sodium

The above theory was used to calculate the AI rate constants  $k_{\text{AI}}$  for the conditions of available experimental studies. Figure 5(a) compares our calculations for  $nP$  states with the data of crossed-beam experiment [12] for  $n = 5-15$ . Figures 5(b)–(d) compare our calculations for  $nP$ ,  $nD$  and  $nS$  states, respectively, with the data of single-beam experiment [2] for  $n = 17-27$ .

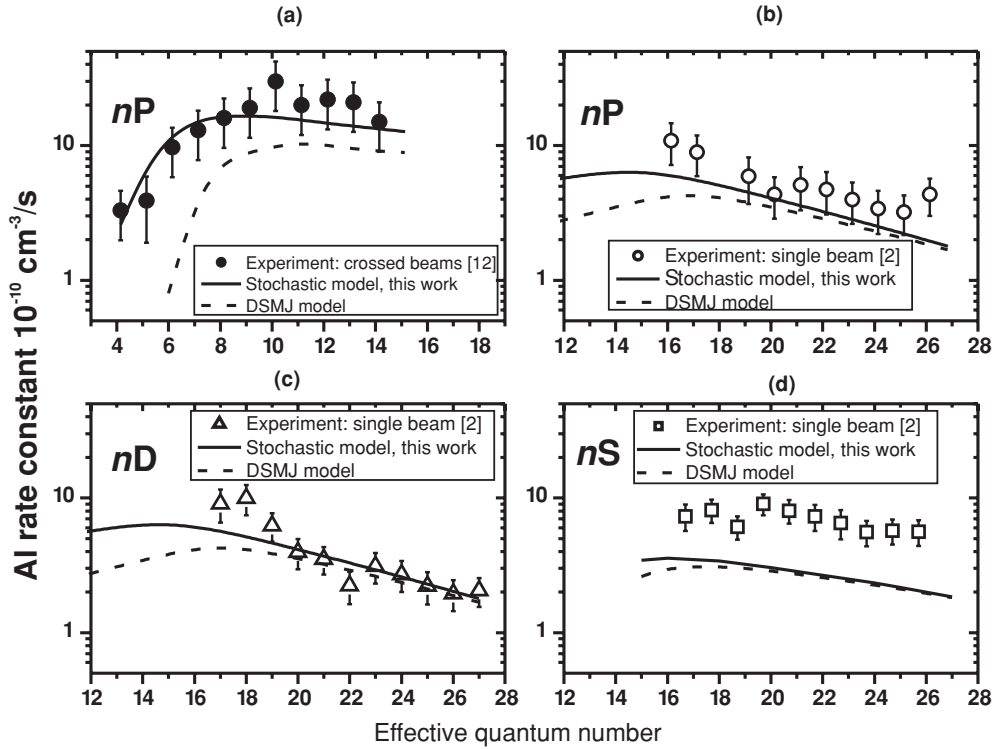


**Figure 5.** Experimental and theoretical  $\text{Na}^{**}(nl) + \text{Na}$  AI rate constants. (a)  $\text{Na}^{**}(nP)$  states, crossed beam conditions [12]; (b)  $\text{Na}^{**}(nP)$  states, single beam conditions [2]; (c)  $\text{Na}^{**}(nD)$  states, single beam conditions [2]; (d)  $\text{Na}^{**}(nS)$  states, single beam conditions [2]; full curves—stochastic model of this work; broken curve—DSMJ model.

In figure 6 our theory is compared with the experimental data of paper I for  $nS$  and  $nD$  states with  $n = 8$ – $20$ . Comparison with another single-beam experiment for  $nP$  states [13] ( $n = 8$ – $15$ ) is given in figure 7. In order to explicitly show the difference between the stochastic and the DSMJ theories, we also give the theoretical results obtained using the nonlinear DSMJ model (broken curves in the figures), in which only the twisting effect is taken into account (see section 2.3). The twisting effect must be taken into account in order to eliminate the divergence of the integral in equation (13) at  $n > 14$  for low-energy head–tail collisions in single atomic beams, while it has almost no effect on the theoretical results in the case of crossed beams.

We used equations (8)–(13), (21) and (22) to calculate individual AI rate constants for different  $l$  quantum numbers. The total  $l$ -mixed rate constants  $k_{\text{AI}}^{\text{mix}}$  were calculated by summing the individual contributions according to equation (43). The effect of population redistribution by BBR was taken into account quantitatively as discussed in section 5.2. Note that the effective ambient temperature of the studies [2, 13] cannot be recovered, because these experiments used liquid nitrogen cooled baffles. Since BBR photons can penetrate the baffles through openings used for the transmission of atomic and laser beams and for the collection of ions and photons, the effective ambient temperature inside the interaction volume is ill-defined. Nevertheless, it should be much lower than the room temperature. We therefore compare these experimental data with calculations performed for 0 K, i.e., no BBR-induced population redistribution.

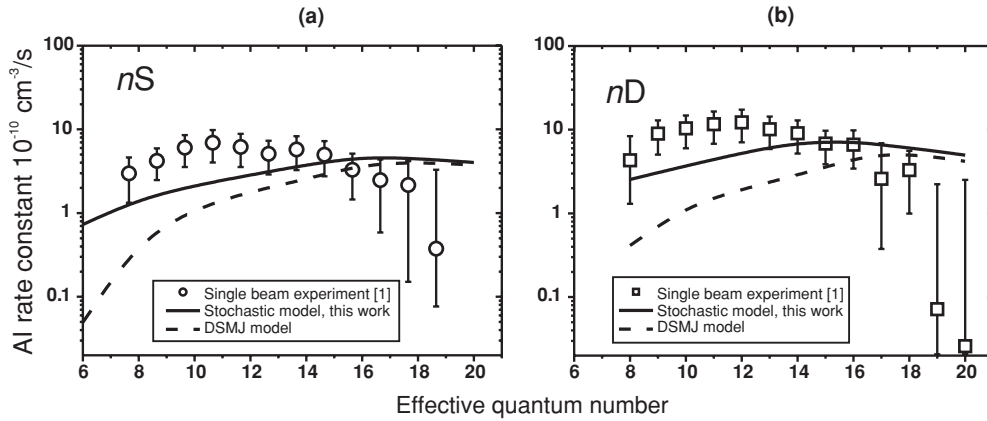


**Figure 6.** Recalculated rate constants of AI in  $\text{Na}^{**}(nS, nD) + \text{Na}$  collisions in a collimated effusive beam from a source at  $T_{\text{bs}} = 635$  K (see discussion in the text). (a) Circles—experiment,  $nS$  states [1]; full curve—stochastic model of this work; broken curve—DSMJ model. (b) Squares—experiment,  $nD$  states [1]; full curve—stochastic model of this work; broken curve—DSMJ model.

When calculating the rate constants for the conditions of the crossed-beam experiment [12], we took into account that the  $\text{Na}_2^+$  ions were produced not only in the collisions of  $\text{Na}^{**}(nl)$  and  $\text{Na}(3S)$  atoms belonging to different beams, but also in head–tail collisions of atoms belonging to the same beam. Due to this fact, the measured rate constant  $k_{\text{AI}}^{\text{exp}}$  is a sum of crossed beam ( $k_{\text{AI}}^{\text{cb}}$ ) and single beam ( $k_{\text{AI}}^{\text{sb}}$ ) rate constants:  $k_{\text{AI}}^{\text{exp}} = k_{\text{AI}}^{\Sigma} = k_{\text{AI}}^{\text{cb}} + k_{\text{AI}}^{\text{sb}}$ .

The full curve in figure 5(a) shows the AI rate constants calculated using the stochastic model for the crossed-beam velocity distribution at  $T_{\text{bs}} = 600$  K given by equation (15). The broken curve is the total AI rate constant calculated using equation (43) and the standard DSMJ model. The results of the stochastic model are in good agreement with the experimental data, while the DSMJ results significantly disagree with them. Figure 5(a) clearly demonstrates that the diffusive migration of the Rydberg electron must be taken into account.

The experimental data at  $T_{\text{bs}} = 1000$  K, shown in figures 5(b)–(d), were not measured in an absolute manner. Instead, the authors of [2] deduced absolute rate constants by adjusting their relative single-beam data for  $nP$  states to the absolute crossed-beam results of [12] for  $n = 15$ –17. Such an approach is not strictly correct, because the collision velocity distributions in single and crossed beams are quite different (see section 2), as has been noted later in [36] by the authors of [2] themselves. Therefore, we treat the experimental rate constants of [2] as relative data, and compare primarily shapes of the experimental and theoretical dependences on  $n_{\text{eff}}$ . Figures 5(b)–(d) show that the shapes of theoretical curves calculated by the stochastic theory are closer to the experimental data than the curves calculated by the DSMJ theory.

Formally one can compare also the absolute rate constant values. A good agreement is observed between the experiment and the theory for  $nD$  states for  $n \geq 20$  in figure 5(c). The agreement for  $nP$  states in figure 5(b) is somewhat worse, while a significant disagreement for  $nS$  states is observed in figure 5(d). The disagreement is most probably explained by incorrect determination of absolute experimental rate constant values in [2]. Such an assumption is confirmed by the observations made in paper I, showing that the AI rate constants for  $nD$  states in single-beam collisions are actually larger than those for  $nS$  states (see figure 6), which is in line with the theoretical predictions of figures 5(c) and (d).

Another interesting observation made in figures 5(b)–(d) is that the results of the stochastic theory and the DSMJ model practically coincide for  $n > 20$ . This can be explained by exponential decrease of the diffusion coefficient (26) with increasing  $R_n$ , whereby the

stochastic theory reduces to the DSMJ model in the limit of no diffusion. It is therefore more important to compare the results of both approaches with the experiments at lower  $n$ , where both models yield significantly different results.

Experiments with  $nS$  and  $nD$  states of Na in the particularly interesting range  $8 \leq n_{\text{eff}} \leq 20$  are reported in paper I. They were performed using a well-collimated (divergence  $< 3^\circ$ ) single effusive atomic beam at the source temperature of 635 K. Paper I concentrated on measurements of the relative dependences of AI rate constants on  $n_{\text{eff}}$ . The absolute rate-constant values were determined by calculating the number density of ground-state atoms from the known geometry of the atomic beam using the widely accepted Nesmeyanov formula [37] to describe the temperature–vapour pressure relation. However, in our more recent examination of the available vapour-pressure data we came to the conclusion that the alternative formula of Browning and Potter [38], which gives approximately two times higher density for the same temperature, is more accurate. This conclusion is based on a careful assessment of the available experimental data, and it is in good agreement with other recent assessments of this question [39]. Therefore the number density of atoms in the beam used in paper I must be increased to  $(5 \pm 1) \times 10^{10} \text{ cm}^{-3}$ . Consequently, the absolute values of experimental AI rate constants reported in paper I must be decreased by about a factor of two before they can be compared with the theory. By doing so, the shapes of the  $k_{\text{AI}}(n_{\text{eff}})$  dependences remain unchanged.

Figure 6 compares the corrected for number density AI rate constants of paper I with the present theoretical results. A reasonable agreement of absolute values between the experimental data and the stochastic model (full curves in figure 6) is observed, while the DSMJ model gives poorer agreement for  $n_{\text{eff}} < 15$  (broken curves in figure 6). At the same time, a noticeable disagreement in the shapes of the experimental and theoretical dependences is found. The experimental dependences have a maximum near  $n_{\text{eff}} = 11, 12$ , which surprisingly coincides with that of the crossed-beam experiment in figure 5(a), while the single-beam theory predicts a maximum near  $n_{\text{eff}} = 17, 18$ . Since the relative dependences of the experimental AI rate constants of paper I were measured under well-controlled and precisely documented conditions, it is reasonable to assume that the observed discrepancies for  $n_{\text{eff}} < 16$  have physical reasons. Two such reasons can be mentioned.

Firstly, velocity distributions in atomic beams are often non-ideal. Special care should be taken to ensure proper conditions for effusion of atoms from the beam source and absence of noticeable scattering and thermalization of atoms in the beam due to intra-beam collisions and collisions with background gases. Such processes change the atomic velocity distribution and mean collision energy, which, in turn, affect the position of the maximum of the experimental dependence  $k_{\text{AI}}(n_{\text{eff}})$ . However, this kind of effect can be disregarded in the case of paper I. The experiment used a well-collimated effusive atomic beam, which was verified by observing the spatial distribution of resonance fluorescence. Furthermore, we measured the absolute velocity distribution of ground-state atoms in the beam using the time-of-flight technique. The relative collision velocity distribution was derived from the measured distribution, and it was found to be very close to that described by equation (16).

Secondly, in the experiments of paper I the collision energies ( $E = 3.1 \times 10^{-4} \text{ au}$ ) were lower than those in the single-beam experiment [2] ( $E = 5.2 \times 10^{-4} \text{ au}$ ) and the crossed-beam experiment [12] ( $E = 2.8 \times 10^{-3} \text{ au}$ ). According to section 4.3 (iii), in these three cases the present stochastic model is applicable for states with  $n_{\text{eff}} > 15$ ,  $n_{\text{eff}} > 12$  and  $n_{\text{eff}} > 7$ , respectively. For lower  $n_{\text{eff}}$  the influence of the chaotic dynamics of the Rydberg electron on the internuclear motion can become non-negligible. The stochastic changes in the quantum state of the Rydberg electron lead to random transitions between the states of the quasi-molecule. This, in turn, causes random changes in forces acting on the colliding

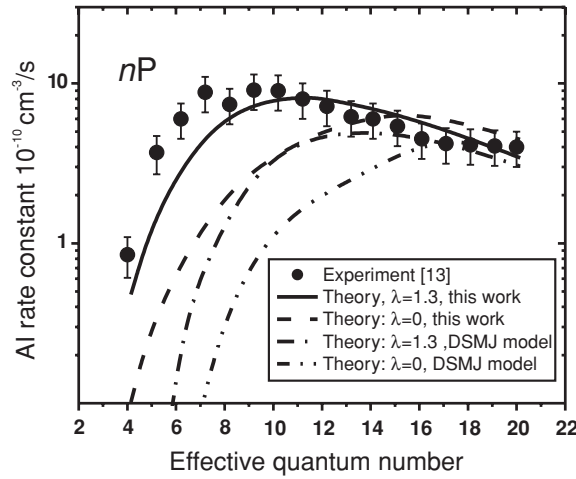


**Figure 7.** Rate constants of AI in Na<sup>\*\*</sup>(*nP*) + Na collisions in a single effusive beam from a source at  $T_{\text{bs}} = 700$  K: circles—experiment [13]; full curve—stochastic model of this work with collimation parameter  $\lambda = 1.3$ ; broken curve—stochastic model with  $\lambda = 0$ ; chain curve—DSMJ model with  $\lambda = 1.3$ ; double dotted chain curve—DSMJ model with  $\lambda = 0$ .

nuclei and may noticeably affect their trajectories if the collisions are sufficiently slow. Such randomization of nuclear motion was disregarded in the present calculations, and it could eventually explain the differences between the experimental and theoretical results, which are seen in figure 6. Therefore, instead of using Newton equations for  $n_{\text{eff}} < 16$ , one should rather treat the nuclear motion in close connection with the dynamics of the Rydberg electron and describe the action of random forces using Langevin-type equations, as is done in the theory of laser-cooled atoms (see, e.g., [40]).

The stochastization can play an important role for relatively low  $n_{\text{eff}} \leq 20$  and relatively low collision energies in single-beam experiments. Under the crossed-beam conditions of [12] this effect is negligible because of the large collision velocities  $\langle v_c \rangle \approx 1100$  m s<sup>-1</sup>. Under the single-beam conditions of [2] ( $\langle v_c \rangle = 480$  m s<sup>-1</sup>) the stochastization of nuclear motion is weak due to the low efficiency of Rydberg electron diffusion for  $n > 20$ . In the case of low energy collisions studied in paper I, the nuclear stochastization should most probably be taken into account. Nevertheless, even if this effect is neglected, the present stochastic model gives closer results to the experimental data than the DSMJ model.

We also compare the theory with another single-beam experiment for *nP* states [13], which was performed under substantially different conditions from those of [1, 2, 12]. This experiment exploited a continuous excitation of Rydberg atoms in a poorly collimated atomic beam at  $T_{\text{bs}} = 700$  K and density by more than an order of magnitude higher than in the other studies. It is possible that the beam used in [13] was not effusive and, hence, its velocity distribution was not properly described by equation (16). As can be shown from the results of [41], the collision velocity distribution of a poorly collimated non-effusive atomic beam can be described by

$$F_{\text{sb}}^{(\lambda)}(v_c) = C_\lambda v_c^\lambda \frac{2.96}{\sqrt{2\pi M T_{\text{bs}}}} \frac{M}{\sqrt{1 + 9\pi M v_c^2 / 128 T_{\text{bs}}}} \exp\left(-\frac{M v_c^2}{T_{\text{bs}}}\right), \quad (50)$$

where  $\lambda$  is a fitting parameter, and  $C_\lambda$  is a normalization constant to be calculated numerically ( $C_{\lambda=0} = 1$ ). The value  $\lambda = 0$  corresponds to an ideal effusive beam, whereas  $\lambda > 0$  takes into account the change of the velocity distribution due to thermalizing collisions.

Figure 7 compares the experimental data of [13] with the theoretical calculations performed using both theoretical models and the velocity distribution (50) with  $\lambda = 0$  and  $\lambda = 1.3$ . When  $\lambda = 0$  ( $\langle v_c \rangle = 400 \text{ m s}^{-1}$ ), both models yield dependences similar to those of figure 6, which disagree with the experiment for lower  $n$ . If the calculations are performed with  $\lambda = 1.3$  ( $\langle v_c \rangle = 680 \text{ m s}^{-1}$ ), the agreement with the experiment substantially improves for the stochastic model (full curve in figure 7), while it remains poor for the DSMJ model (chain curve in figure 7).

Note that using the velocity distribution given by equation (50) for improvement of the agreement with the experimental data of paper I (figure 6) is not reasonable. The value  $\lambda = 1.3$  corresponds to a beam with a divergence angle of about  $40^\circ$ , while the divergence angle of the beam used in paper I was one order of magnitude smaller. Small values of  $\lambda < 0.2$  have practically no effect on the calculated AI rate constants. We therefore conclude that the stochastic theory of collisional ionization works well in the case of thermal collisions in crossed beams, and the same can be expected under vapour cell conditions. However, it must be further developed in order to properly describe the collisions for  $n < 17$  at sub-thermal energies in single beams.

## 6. Conclusion

In this study, we have proposed an essential improvement of the DSMJ model describing the ionization processes in collisions of Rydberg atoms with ground-state atoms. The following effects have been taken into account: (1) variation of the collision velocity distributions in single- and crossed-beam experiments; (2) nonlinearity of basic equations of the DSMJ model; (3) collisional  $l$ -mixing, which occurs to  $nP$  and  $nD$  atoms prior to associative ionization; (4) ‘twisting’ of the colliding atoms in attractive potentials due to the polarization of atoms; (5) mixing of Rydberg states due to the BBR-induced and spontaneous transitions; (6) diffusion of the Rydberg electron through its energy spectrum during the collision. Inclusion of the latter effect is the most substantial modification of the DSMJ model. Non-adiabatic processes in the region of overlapping level crossings, which are characteristic for the quasi-molecular manifold of Rydberg states, were modelled using the stochastic theory, which allowed us to take into account the stochastic dynamics of the Rydberg electron.

Comparison of the results of the stochastic theory with the data of crossed-beam experiments for  $nP$  states with  $n = 5$ –15 at relatively large collision energies shows a good quantitative agreement. A good qualitative agreement with the data of single-beam experiments for  $nS$ ,  $nP$ ,  $nD$  states with  $n = 17$ –27 is also seen, and satisfactory agreement is found for  $n = 8$ –16. We have shown that the developed stochastic model yields a significantly improved agreement with the results of single- and crossed-beam experiments, as compared to other theoretical approaches. At the same time, the stochastic model requires further development in order to account for possible correlation effects between electronic and nuclear degrees of freedom in sub-thermal energy collisions. Such effects are expected to play an important role in slow atomic collisions. The third (final) part of this study [42] will assess the validity of the above reasoning by performing experimental and theoretical studies of ionization of  $\text{Na}(nS)$  and  $\text{Na}(nD)$  atoms in crossed atomic beams.

## Acknowledgments

This work was supported by INTAS grant no 2001-155, INTAS Young Scientist Fellowship No 04-83-3692, Russian Foundation for Basic Research grants no 05-02-16181 and no

05-03-33252, NATO grant no EAP.RIG.981378, EU TOK project LAMOL, Latvian Science Council, Deutsche Forschungsgemeinschaft, European Social Fund and Russian Science Support Foundation.

## References

- [1] Ryabtsev I I, Tretyakov D B, Beterov I I, Bezuglov N N, Miculis K and Ekers A 2005 *J. Phys. B: At. Mol. Phys.* **38** S17
- [2] Weiner J and Boulmer J 1986 *J. Phys. B: At. Mol. Phys.* **19** 599
- [3] Duman E L and Shmatov I P 1980 *Sov. Phys.—JETP* **51** 1061
- [4] Janev R K and Mihajlov A A 1980 *Phys. Rev. A* **21** 819
- [5] Mihajlov A A and Janev R K 1981 *J. Phys. B: At. Mol. Phys.* **14** 1639
- [6] Weiner J, Masnou-Seeuws F and Giusti-Suzor A 1990 *Adv. At. Mol. Opt. Phys.* **26** 209
- [7] Klucharev A N and Vujnovic V 1990 *Phys. Rep.* **185** 55
- [8] Nikitin E E and Umansky S Ya 1984 *Theory of Slow Atomic Collisions* (New York: Springer)
- [9] Bezuglov N N, Borodin V M, Kazanskii A K, Klyucharev A N, Matveev A A and Orlovskii K V 2001 *Opt. Spectrosc.* **91** 19
- [10] Bezuglov N N, Borodin V M, Ekers A and Klyucharev A N 2002 *Opt. Spectrosc.* **93** 661
- [11] Bezuglov N N, Borodin V M, Grushevski V, Klyucharev A N, Michulis K, Fuso F and Allegrini M 2003 *Opt. Spectrosc.* **95** 515
- [12] Boulmer J, Bonanno R and Weiner J 1983 *J. Phys. B: At. Mol. Phys.* **16** 3015
- [13] Zagrebin S B and Samson A V 1985 *J. Phys. B: At. Mol. Phys.* **18** L217
- [14] Muller W and Meyer W 1984 *J. Chem. Phys.* **80** 3311
- [15] Nikitin E and Smirnov B 1978 *Sov. Phys.—Usp.* **21** 95
- [16] Bezuglov N N, Klyucharev A N and Sheverev V A 1987 *J. Phys. B: At. Mol. Phys.* **20** 2497
- [17] Bezuglov N N, Borodin V M, Klyucharev A N, Orlovsky K V and Allegrini M 1997 *Opt. Spectrosc.* **82** 334
- [18] Zaslavsky M G 1998 *Physics of Chaos in Hamiltonian Systems* (River Edge, NJ: Imperial College Press)
- [19] Reichl L E 1992 *The Transition to Chaos In Conservative Classical Systems: Quantum Manifestations* (New York: Springer)
- [20] Matrasulov D U 1999 *Phys. Rev. A* **60** 700
- [21] Benvenuto F, Casati G and Shepelyansky D L 1996 *Phys. Rev. A* **53** 737
- [22] Delone N B, Zon B A and Krainov V P 1978 *Sov. Phys.—JETP* **48** 223
- [23] Beigman I L and Lebedev V S 1995 *Phys. Rep.* **250** 95
- [24] Jensen R V, Susskind S M and Sanders M M 1991 *Phys. Rep.* **201** 1
- [25] Delone N B, Krainov V N and Shepelyansky D L 1983 *Sov. Phys.—Usp.* **26** 551
- [26] Gontis V and Kaulakys B 1987 *J. Phys. B: At. Mol. Phys.* **20** 5051
- [27] Bezuglov N N and Borodin V M 1999 *Opt. Spectrosc.* **86** 467
- [28] Kaulakys B and Ciziunas A 1987 *J. Phys. B: At. Mol. Phys.* **20** 1031
- [29] Kramers H A 1940 *Physica* **7** 284
- [30] Dashevskaja E I, Litvin I, Nikitin E E, Oref I and Troe J 2000 *Phys. Chem. Chem. Phys.* **2** 2251
- [31] Weisskopf V 1933 *Z. Phys.* **34** 1  
Weisskopf V 1933 *Z. Phys.* **34** 451
- [32] Lebedev V S and Marchenko V S 1986 *Sov. Phys.—JETP* **64** 251
- [33] Lifshitz E M and Pitayevsky L P 1980 *Physical Kinetics* (Oxford: Pergamon)
- [34] Kaulakys B 1991 *J. Phys. B: At. Mol. Opt. Phys.* **24** L127
- [35] Sobel'man I I 1992 *Atomic Spectra and Radiative Transitions* (Berlin: Springer)
- [36] Wang M W and Weiner J 1988 *J. Phys. B: At. Mol. Opt. Phys.* **21** L15
- [37] Nesmeyanov A N 1963 *Vapour Pressure of the Chemical Elements* (Amsterdam: Elsevier)
- [38] Browning P and Potter P E 1985 An assessment of the experimentally determined vapour pressures of the liquid alkali metals *Handbook of Thermodynamic and Transport Properties of Alkali Metals* (Boston, MA: IUPAC, Blackwell Scientific Publications) chapter 6.2
- [39] Bystrov P I, Kagan D N, Krechetova G A and Shpil'rain E E 1990 *Liquid-Metal Coolants for Heat Pipes and Power Plants* (New York: Hemisphere)  
Vargaftik N B and Voljak L D 1985 Thermodynamic properties of alkali metal vapours at low pressures *Handbook of Thermodynamic and Transport Properties of Alkali Metals* (Boston, MA: IUPAC, Blackwell Scientific Publications) chapter 6.6.1

- Fink J K and Leibowitz L 1979 Thermophysical properties of sodium *Argonne National Laboratory Report, ANL-CEN-RSD-79-1*
- Thurnay K 1981 Thermophysical properties of sodium in the liquid and gaseous states *Kernforschungszentrum Karlsruhe GmbH Report, KfK 2863*
- [40] Javanainen J 1992 *Phys. Rev. A* **46** 5819
- [41] Bezuglov N N, Vuinovich V, Klyucharev A N and Sheverev V A 1989 *Opt. Spectrosc.* **66** 721
- [42] Beterov I I, Tretyakov D B, Ryabtsev I I, Bezuglov N N, Miculis K and Ekers A 2005 *J. Phys. B: At. Mol. Opt. Phys.* to be submitted